Influence of the microstructure and voids on the high-cycle fatigue strength of 316L stainless steel under multiaxial loading

Raphaël Guerchais, Franck Morel, Nicolas Saintier, Camille Robert

doi: 10.1111/ffe.12304

Influence of the microstructure and voids on the high-cycle fatigue strength of 316L stainless steel under multiaxial loading

R. GUERCHAIS[1,2], F. MOREL[1], N. SAINTIER[2] and C. ROBERT[1]

[1]*LAMPA, Arts et Métiers ParisTech, 49035 Angers Cedex 01, France,* [2]*I2M, Arts et Métiers ParisTech, Esplanade des Arts et Métiers, 33405 Talence, France*

ABSTRACT In the present study, the effects of both the microstructure and voids on the high-cycle fatigue behaviour of the 316L austenitic stainless steel are investigated by using finite element simulations of polycrystalline aggregates. The numerical analysis relies on a metallurgical and mechanical characterization. In particular, fatigue tests are carried out to estimate the fatigue limits at 2.10^6 cycles under uniaxial and multiaxial loading conditions (combined tension and torsion and biaxial tension) using both smooth specimens and specimens containing an artificial hemispherical defect. The simulations are carried out with several configurations of crystalline orientations in order to take into account the variability of the microstructure in the predictions of the macroscopic fatigue limits. These predictions are obtained, thanks to a probabilistic fatigue criterion using the finite element results. The capability of this criterion to predict the influence of voids on the average and the scatter of macroscopic fatigue limits is evaluated.

Keywords 316L austenitic steel; cubic elasticity; defect; high-cycle fatigue; multiaxial loadings; polycrystalline aggregate; probabilistic fatigue criterion.

NOMENCLATURE

$\langle \bullet \rangle_a$	=	volume-weighted average over the polycrystalline aggregate
$\langle \bullet \rangle_g$	=	volume-weighted average over the grain
$a = \frac{2C_{1212}}{C_{1111}-C_{1122}}$	=	Zener anisotropy factor
$k_{\theta z} = \Sigma_{\theta z}/\Sigma_{zz}$	=	biaxiality ratio in tension–torsion
$k_{\theta\theta} = \Sigma_{\theta\theta}/\Sigma_{zz}$	=	biaxiality ratio in biaxial tension
$\underline{l}$	=	unit vector normal to the slip plane (Fig. 1a)
$\underline{n}^s$	=	unit vector in the slip direction (Fig. 1a)
$R = \Sigma_{ij,min}/\Sigma_{ij,max}$	=	loading ratio
s_{-1}	=	macroscopic average fatigue limit under fully reversed tension
T	=	period of the loading cycle
t_{-1}	=	macroscopic average fatigue limit under fully reversed torsion
$\varphi_{\theta z}$	=	phase shift in tension–torsion
$\varphi_{\theta\theta}$	=	phase shift in biaxial tension
$\underline{\underline{\Sigma}} = \left\langle \underline{\underline{\sigma}} \right\rangle_a$	=	macroscopic stress tensor
$\left\langle \underline{\underline{\sigma}} \right\rangle_g$	=	mesoscopic stress tensor
$\underline{\sigma}_n\left(\underline{n}, t\right)$	=	mesoscopic normal stress vector (Fig. 1b)
$\sigma_{n,a}$	=	mesoscopic normal stress amplitude

Correspondence: R. Guerchais. E-mail: guerchais@lms.polytechnique.fr

$\sigma_{n,m}$ = mesoscopic mean normal stress

$\underline{\tau}(\underline{n}, t)$ = mesoscopic shear stress vector (Fig. 1b)

τ_a = mesoscopic shear stress amplitude (Fig. 1b)

INTRODUCTION

The present study is dedicated to the high-cycle fatigue (HCF) strength of a 316L austenitic stainless steel, in the presence of small defects and under multiaxial loadings. The defects considered in this work are artificial voids, with a low sharpness and dimensions close to the mean grain size. As the stress concentrations induced by such voids may favour the fatigue crack initiation, the evaluation of their influence on the fatigue strength is crucial for design purposes. A thorough review of fatigue criteria predicting the effect of defects on the fatigue limit under fully reversed uniaxial tension was conducted by Murakami and Endo.[1] The authors present a classification of these criteria in three categories (empirical models, models based on the stress concentration factor and models based on fracture mechanics) and provide a detailed assessment of their performances and procedure to identify and apply these criteria. Auricchio *et al.* have shown the relevancy of a volumetric approach combined with an energy-based criterion to assess the fatigue life of 316L steel notched components.[2] Furthermore, several authors have proposed fatigue criteria taking into account accurately the detrimental influence of defects on the fatigue limits in other macroscopic loading conditions, for example, in torsion[3] and in combined tension and torsion.[4] However, although the practical interest of these approaches, which relies either on the fracture mechanics or the theory of critical distance,[5] is undeniable, they often involve a material characteristic length whose meaning is unclear: sometimes a physical explanation is invoked, whereas other times this length is associated with a microstructural length. Besides, some of them do not allow to account for complex defect geometries. Moreover, these methods evade the issue of the scatter of the fatigue strength.

The present work aims to analyse the competition existing between the stress concentration or stress heterogeneity induced by a small void and the one induced by the anisotropic elastic behaviour of the grains in order to determine at which defect size the void effect takes over the natural heterogeneity at the local scale, thus conditioning the fatigue strength of the polycrystal. The second objective is to assess if the variability and lack of representativeness of crystal orientations in the vicinity of a void may affect the scatter of the fatigue limit. To address these issues, a numerical study using finite element (FE) simulations of polycrystalline aggregate is carried out. This kind of numerical simulations, in which polycrystalline microstructures are explicitly modelled, has been used in several recent studies dealing with HCF issues. For instance, Bennett and McDowell[6] have analysed the distribution of fatigue crack initiation parameters (FIP) inspired from well-known HCF criteria and have attempted to predict the distribution of fatigue crack lengths in a polycrystal using a crack growth law based on the FIP. This study was enriched by the work of Guilhem *et al.*[7] in which the mechanical response of the grains is studied according to their positions in the aggregate, their orientations and those of the neighbouring grains. Moreover, FE simulations of polycrystalline aggregates have recently been used to study the influence of defects on the HCF strength. For example, the effect of a rough surface on the distribution of some mechanical

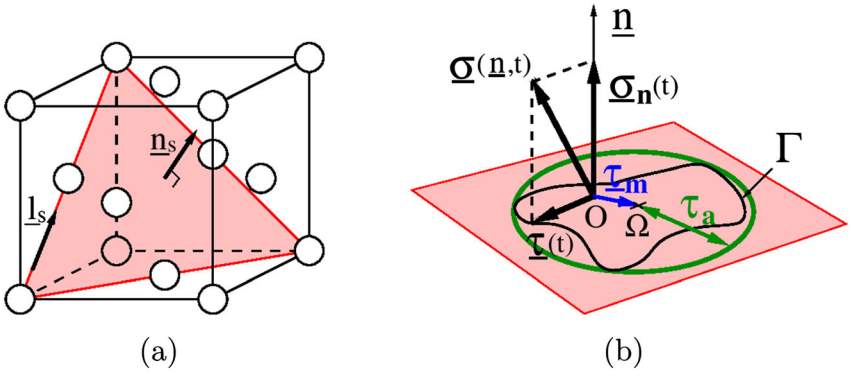

Fig. 1 Representation of some mechanical quantities and vectors in (a) a face-centred cubic unit cell and (b) a slip plane.

quantities has been investigated,[8,9] and the influence of the defect size and sharpness has been extensively studied by Owolabi *et al.* in the case of semicircular notches,[10] under uniaxial loading conditions.

In the present case, the results of the FE simulations of polycrystalline aggregate allow to evaluate the mechanical quantities used in a probabilistic fatigue criterion. The probabilistic approaches offer a convenient framework to assess the scatter of the fatigue strength or life as shown, for example, in a recent study conducted by Charkaluk *et al.* on a porous steel in low cycle fatigue regime.[11] The methodology followed in this paper has been applied in previous studies dealing with an electrolytic copper.[12,13] In these works, the capability of the probabilistic fatigue criterion to satisfactorily predict the average fatigue limit has been shown, but the issues of small defects and of multiaxial loadings were studied separately because of the lack of experimental data. Nevertheless, it can be essential to make sure of the relevancy of the predictions in complex conditions involving both small defects and multiaxial loadings because some applications can face with these two aspects. For instance, some medical implants, like stents,[14,15] undergo multiaxial cyclic loadings and stress concentrations comparable with those induced by the voids considered in this study. This is why these two aspects are dealt with jointly in the present study, by relying on an experimental characterization of the 316L austenitic steel. Uniaxial HCF tests have already been carried out by Wiersma and Taylor[16] and Donnelly[17] on a 316L austenitic steel using smooth and notched specimens. However, because of the lack of experimental data on the fatigue strength under multiaxial loading conditions, a series of fatigue tests is conducted, in the present study, on specimens including a hemispherical artificial void for a large range of void sizes and loading conditions, thus allowing to confront the fatigue limits predicted by the probabilistic fatigue criterion to those estimated experimentally and to define the validity domain of the probabilistic criterion.

EXPERIMENTAL MULTIAXIAL FATIGUE TESTS

Characterization of 316L austenitic stainless steel

The austenitic stainless steel American Iron and Steel Institute (AISI) 316L studied in this work is produced by Aubert & Duval and commercially named 316L M25W. It is provided in the form of round bars with a diameter of 40 mm and a length of 1.2 m. The chemical composition of this AISI 316L, determined by spark atomic emission spectrometry and presented in Table 1, is designed to provide a ferrite-free microstructure. Moreover, the martensitic transformation, which could occur during the heat treatment or the mechanical loading, is prevented, thanks to a high percentage of nickel, thus ensuring a purely austenitic structure (i.e. constituted by face-centred cubic crystals). Because of a large proportion of chromium and nickel, the material does not exactly observe the AISI 316L grade, but for simplicity, it will still be named 316L in the following.

Table 1 Chemical composition of 316L M25W steel

Elements	C	Cr	Ni	Mo	Mn
Wt%	0.02	19.0	15.0	3.0	1.9

Electron backscatter diffraction (EBSD) analyses are conducted in order to characterize the grains morphology of this 316L austenitic steel. Two sections of the bar are analysed: the sections perpendicular to the axial and orthoradial directions. These analyses are performed in the regions corresponding to the location of the gauge section of the fatigue test specimen. It has been observed that the grain morphology is almost equiaxed, with a mean grain size, defined as the square root of the mean area of the grain and including the twin boundaries, equal to 14 μm in the section perpendicular to the axial direction and 13 μm in the section perpendicular to the orthoradial direction.

Finally, the crystallographic texture of the material is determined by X-ray diffraction using a Seifert XRD3000 diffractometer with a chromium anode. The region of the bar that is analysed corresponds to the location of the gauge section of the fatigue test specimen. The diffracting planes used are the planes {111}, {200} and {220}. The intensities measured on the specimen I_{spe} during the X-ray diffraction analysis are corrected in two steps: the average background noise is deleted from the intensities I_{spe}, then these corrected intensities I_{spe} are normalized by the intensities I_{ref} measured on a 316L steel powder, that is, a non-textured sample. After these corrections, the intensities are then treated by MTEX,[18] a MATLAB® Toolbox for quantitative texture analysis, in order to determine the continuous orientation density function. It appears from these results that the 316L austenitic steel studied is weakly textured.

The usual mechanical properties of the 316L steel are obtained from a tensile test and are presented in Table 2, namely the Young modulus E, the Poisson ratio ν, the yield stress $R_{p0.2\,\%}$ defined at a plastic strain of 0.2% and the tensile strength R_m.

Table 2 Tensile properties of AISI 316L M25W steel

E (GPa)	ν	$R_{p0.2\,\%}$ (MPa)	R_m (MPa)
194	0.284	346	644

Fatigue tests conditions

The objective is to estimate the average fatigue limits, defined at 2.10^6 cycles, of the 316L austenitic steel under several loading conditions and for various void sizes. Fatigue tests are carried out at room temperature, in an air environment and at a frequency of 10 Hz on an Instron 8850 servohydraulic fatigue testing machine (Instron, Norwood, Massachusetts, USA). In addition to its capacity to exert an axial force and a torque, the Instron 8850 allows applying a cyclic uniform pressure on the internal surface of the gauge of a tubular specimen. This pressure leads to an almost uniaxial stress state characterized by an orthoradial normal stress $\Sigma_{\theta\theta}$. The stress state is not exactly uniaxial because of the radial normal stress Σ_{rr} induced by the internal pressure P. More precisely, the radial normal stress Σ_{rr} is heterogeneously distributed along the gauge thickness and decreases from $-P$ to 0 between the internal surface and the external surface. Thus, the maximum ratio between the radial and the orthoradial normal stresses is located at the internal surface and is approximately equal to 15%. It should also be noted that the orthoradial normal stress $\Sigma_{\theta\theta}$ is not constant along the gauge thickness. Indeed, considering an isotropic elastic behaviour in the gauge section, the gradient of the orthoradial normal stress from the internal surface to the external surface is in average equal to $-0.59\,P$ MPa mm^{-1}. It is worth noting that, even though the hydrostatic stress is equivalent between the two free surfaces, the shear stress is larger at the internal surface. Thus, in plain specimens, the fatigue crack initiation is likely to occur on this surface. On the contrary, in specimens containing a void, the fatigue cracks are more likely to occur on the external surface. In any cases, whatever the loading condition considered, FE simulations including an elasto-plastic model are systematically used to determine the macroscopic stress state at the location of the fatigue crack initiation observed experimentally, excepted for one specimen with a void diameter $D = 365$ µm and loaded in biaxial tension because of an unexpected initiation on the internal surface. Moreover, the results are expressed in terms of nominal macroscopic stress; that is, the defect is neglected in the FE simulations used for the determination of the stress states, as it is commonly performed.

Six loading conditions are studied:

- uniaxial tension with a loading ratio $R = -1$;
- torsion with a loading ratio $R = -1$;
- in-phase uniaxial tension and torsion with a loading ratio $R = -1$ and a biaxiality ratio $k_{\theta z} = 0.5$;
- out-of-phase uniaxial tension and torsion with a loading ratio $R = -1$, a biaxiality ratio $k_{\theta z} = 0.5$ and a phase shift $\varphi_{\theta z} = 90°$;
- uniaxial tension with a loading ratio $R = 0.1$; and
- in-phase biaxial tension with a loading ratio $R = 0.1$ and a biaxiality ratio $k_{\theta\theta} = 0.5$.

The shape and dimensions of the tubular specimens used for the fatigue tests are presented in Fig. 2. The external gauge section of the specimen is polished up to 6 µm diamond on low napped cloths. In order to study the influence of voids on the fatigue strength, fatigue tests are carried out using specimens containing an artificial void and plain (defect-free) specimens. The artificial defect geometry chosen in these works is hemispherical. This void is introduced by sinker electric discharge machining, using tungsten electrodes, in a flat surface polished on the gauge section of the specimens (Fig. 3a). The flat surface is obtained by successive polishing, using silicon carbide abrasive papers and synthetic nap cloths impregnated with 3 µm diamond suspension, to obtain a mirror finish. For each loading condition, both smooth specimens and specimens containing an artificial

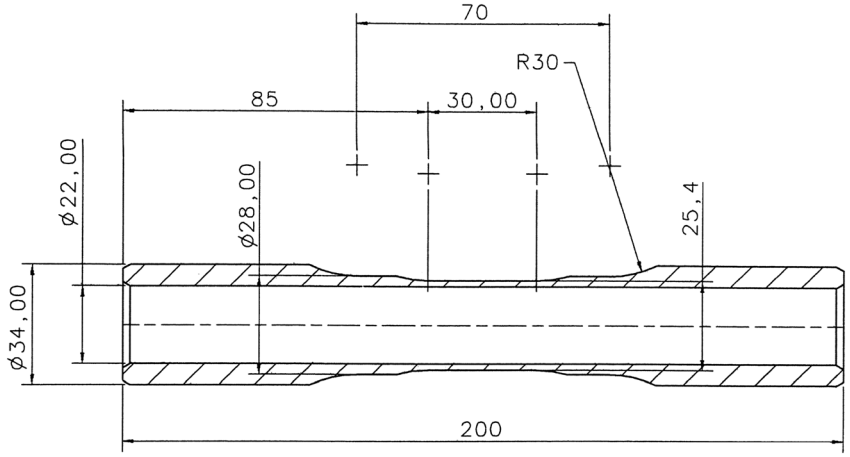

Fig. 2 Shape and dimensions of tubular fatigue test specimen (all dimensions are in millimetre).

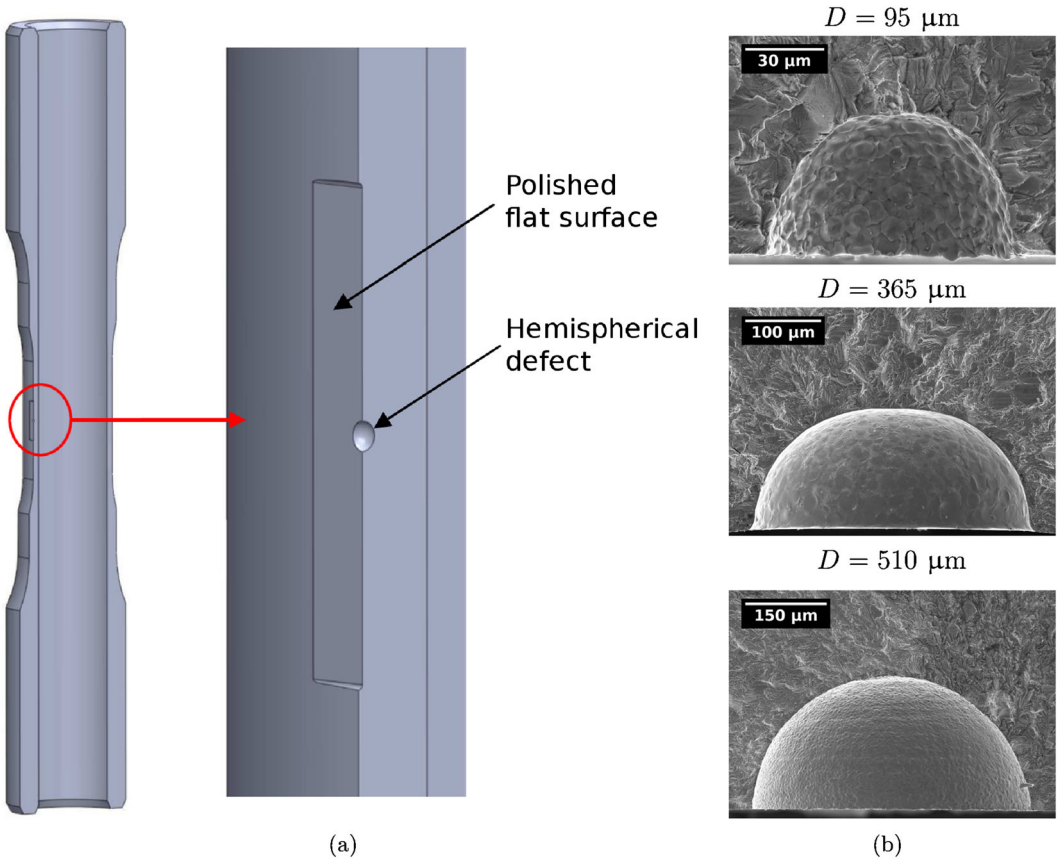

Fig. 3 (a) Cutaway view of the specimen and magnified view highlighting the hemispherical defect introduced in a flat surface polished on the gauge section and (b) examples of fracture surfaces illustrating the shape of the hemispherical defect for different defect diameters, introduced in the fatigue test specimens.

hemispherical void with a diameter $D = 365\,\mu m$ are tested. In addition, in the cases of the fully reversed tension and fully reversed torsion, two other defect diameters D are considered: 95 and 510 µm. The fracture surfaces presented in Fig. 3b illustrate the shape of the hemispherical void for each defect diameter studied.

The objective here is not to precisely determine the average fatigue limits defined at 2.10^6 cycles but to obtain satisfactory estimations of these fatigue limits. Thus, only a limited number of specimens have been prepared in these experiments. More precisely, three specimens are used per configuration (defect size and loading condition). The method consists in applying successively on a specimen, increasing loading blocks of constant stress amplitude during 2.10^6 cycles. If the specimen sustains 2.10^6 cycles, at a given stress amplitude, without initiation of a fatigue crack, then another loading stage at a higher stress amplitude is applied during 2.10^6 cycles and so on, until the failure of the specimen is reached. This procedure is based on the hypothesis that the loading blocks preceding the last stage (i.e. the loading block leading to the failure of the specimen) does not affect the fatigue strength. In other words, it is assumed that neither damage nor strengthening occurs when the loading amplitude is below the fatigue limit defined at 2.10^6 cycles.

The average fatigue limits are estimated from these results by averaging, for each component Σ_{ij} of the macroscopic stress tensor $\underline{\underline{\Sigma}}$, two stress amplitudes:

- $\Sigma_{ij,a}^{NF}$ corresponding to the maximal amplitude tested for which no fatigue crack has been observed after 2.10^6 cycles of loading; and
- $\Sigma_{ij,a}^{F}$ corresponding to the minimal amplitude tested for which no specimen sustained 2.10^6 cycles of loading.

Results and discussion of the fatigue tests

The results of the fatigue tests in fully reversed combined tension and torsion, including fully reversed tension and fully reversed torsion, are gathered in a diagram $\Sigma_{ij,a}$–D in Fig. 4a, and the estimated average fatigue limits are presented in Table 3. The macroscopic stress amplitude $\Sigma_{ij,a}$ corresponds to $\Sigma_{zz,a}$ in the cases of fully reversed tension and fully reversed combined tension and torsion, whereas it corresponds to $\Sigma_{\theta z,a}$ in the case of fully

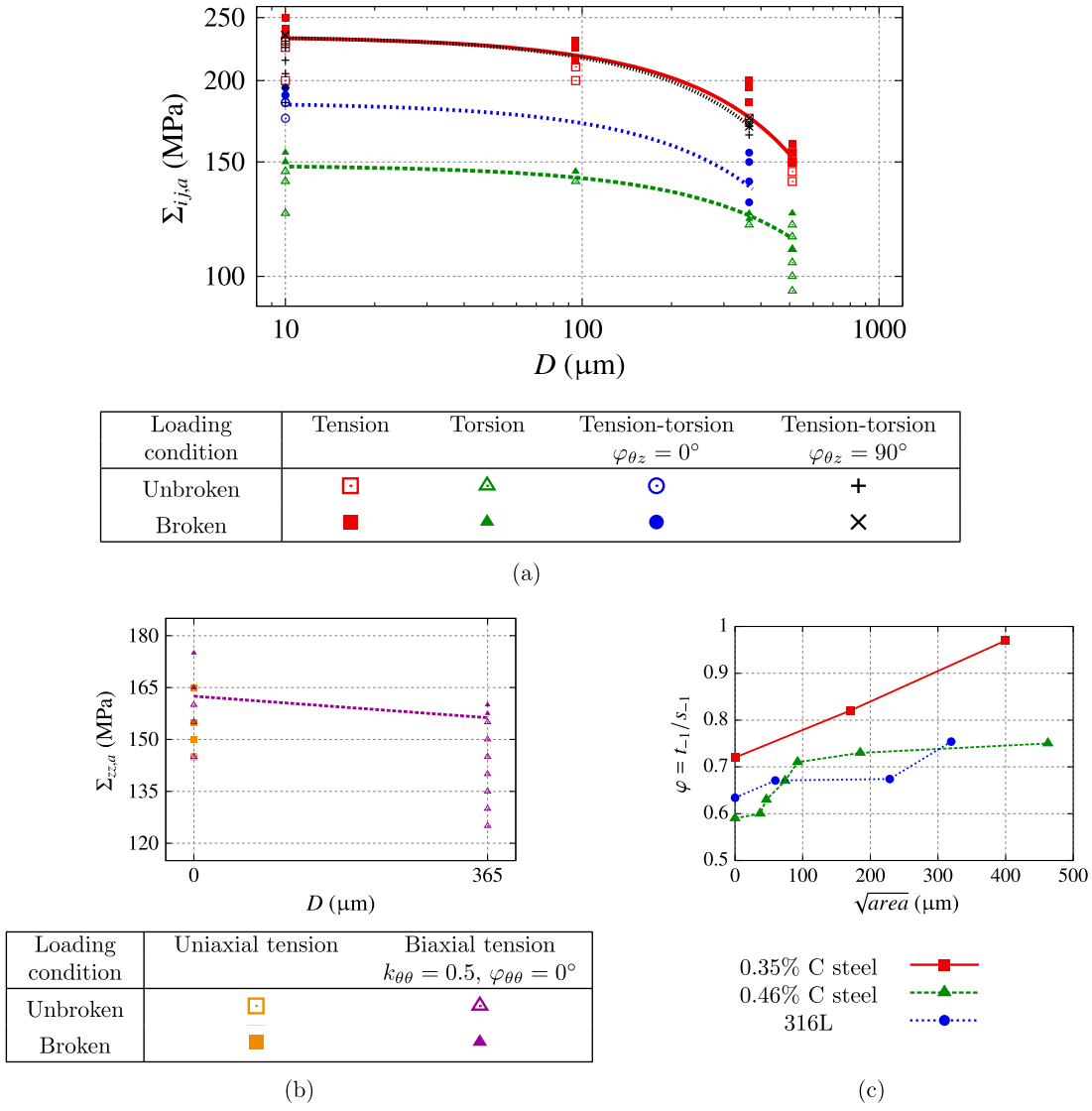

Fig. 4 Results of the fatigue tests conducted on the 316L steel (a) in uniaxial tension and torsion with a loading ratio $R = -1$ and (b) in uniaxial tension and biaxial tension with a loading ratio $R = 0.1$ and (c) evolution of the ratio ϕ between the fatigue limits in torsion and in uniaxial tension as a function of the defect diameter D for different steels.

reversed torsion. In this diagram, the filled symbols represent fatigue test conditions for which a specimen broke before 2.10^6 cycles, and the hollow symbols represent fatigue test conditions for which a specimen sustained the cyclic loading during 2.10^6 cycles. The dashed lines illustrate schematically the evolution of the average fatigue limit depending on the void diameter D for each loading conditions.

This figure clearly shows the beneficial effect of the increase in the phase shift $\varphi_{\theta z}$ from 0° to 90°, on the fatigue strength in the case of a combined tension and torsion loading with a biaxiality ratio $k_{\theta z} = 0.5$. Indeed, the addition of a shear stress amplitude $\Sigma_{\theta z,a}$ does not lead to a decrease of the admissible normal stress amplitude $\Sigma_{zz,a}$ when $\varphi_{\theta z} = 90°$, while a significant drop in this admissible stress amplitude $\Sigma_{zz,a}$ is observed when the shear stress $\Sigma_{\theta z}$ is acting in phase with the normal stress Σ_{zz}. For this loading condition, the decrease in the admissible stress amplitude $\Sigma_{zz,a}$ is approximately 20% for smooth specimens and 30% for specimens containing a void with a diameter $D = 365$ μm.

Another important conclusion, which can be drawn from these fatigue tests, is that, whatever the loading condition considered, the curves do not show a clearly defined critical defect size, that is, a defect size under which the fatigue strength is not affected by the void, contrary to the observations of Endo and Murakami on the 0.46% C steel.[19] Moreover, the slope of the fatigue crack initiation threshold in a Kitagawa–Takahashi diagram ($\log(\Sigma_{ij,a})$ versus $\log(D)$) is not equal to $-1/6$.

Table 3 Average fatigue limits estimated from the fatigue tests

Loading condition	D (μm)	$\Sigma_{ij,a}$ (MPa)					
		$\Sigma_{zz,a}$	$\Sigma_{zz,m}$	$\Sigma_{\theta z,a}$	$\Sigma_{\theta z,m}$	$\Sigma_{\theta\theta,a}$	$\Sigma_{\theta\theta,m}$
Uniaxial tension $R=-1$	0	233	0	0	0	0	0
	95	213	0	0	0	0	0
	365	180	0	0	0	0	0
	510	153	0	0	0	0	0
Torsion $R=-1$	0	0	0	148	0	0	0
	95	0	0	143	0	0	0
	365	0	0	121	0	0	0
	510	0	0	115	0	0	0
Tension–torsion $R=-1$, $k_{\theta z}=0.5$, $\varphi_{\theta z}=0°$	0	188	0	94	0	0	0
	365	120	0	60	0	0	0
Tension–torsion $R=-1$, $k_{\theta z}=0.5$, $\varphi_{\theta z}=90°$	0	233	0	116	0	0	0
	365	169	0	84	0	0	0
Biaxial tension $R=-1$, $k_{\theta\theta}=0.5$, $\varphi_{\theta\theta}=0°$	0	163	199	0	0	81	99
	365	157	193	0	0	79	96
Uniaxial tension $R=0.1$	0	148	180	0	0	0	0

Hence, the trends observed on the 316L steel do not match to those suggested by Susmel and Taylor,[3] relying on the results of Endo and Murakami.[19] In these conditions, it can be more relevant to study the ratio φ between the fatigue limits under fully reversed torsion t_{-1} and fully reversed tension s_{-1} (Eq. 1) versus the void size in order to identify a common feature between the experimental data found in the literature:

$$\varphi = t_{-1}/s_{-1}. \tag{1}$$

To compare the results obtained with different geometries of defect, an equivalent geometrical parameter is required. Because of its widespread applications and convenience, the parameter $\sqrt{area}$ proposed by Murakami and Endo[1,20] is chosen. This parameter is defined as the square root of the area obtained by projecting the void on the plane perpendicular to the maximum principal stress direction. The evolution of the ratio φ as a function of the parameter $\sqrt{area}$ is represented in Fig. 4c and is compared with those observed by Endo and Murakami on a 0.46% C steel,[19] and by Billaudeau *et al.* on a 0.35% C steel.[21] It appears that the influence of the void is more detrimental in fully reversed tension than in fully reversed torsion. Indeed, for each steel considered, the ratio φ increases with increasing defect size $\sqrt{area}$.

The results of fatigue tests in biaxial tension with a loading ratio $R=0.1$, including the uniaxial tension that corresponds to the case where $k_{\theta\theta}=0$, are gathered in a diagram $\Sigma_{ij,a}$–D in Fig. 4b, and the estimated average fatigue limits are presented in Table 3. From these results, it appears that an increase of the biaxiality ratio $k_{\theta\theta}$, from 0 to 0.5, has a beneficial effect on the fatigue strength. Indeed, the addition of an in-phase macroscopic stress amplitude $\Sigma_{\theta\theta,a}$ leads to increase the admissible stress amplitude $\Sigma_{zz,a}$ by 10%. It is worth noting that the capacity of some fatigue criteria to predict this favourable effect has been previously reported.[12]

In addition, under the investigated biaxial tension condition, it can be observed that a hemispherical void with a diameter $D=365$ μm only slightly affects the fatigue strength in comparison with the case without defect. Indeed, the average fatigue limit only decreases by 3% for a void diameter D varying from 0 to 365 μm. By way of comparison, the decrease in the fatigue limit under fully reversed tension is about 23% between the smooth specimen and the specimen containing a void with a diameter $D=365$ μm.

In the case of defect-free specimen, the initiation site depends on the loading condition. Indeed, for uniaxial and biaxial tension loadings, fatigue cracks initiate preferentially on the internal free surface because of small scratches. On the contrary, in the case of loading condition including torsion, the initiation occurs on the external surface. Indeed, because of a larger macroscopic shear stress at the external surface than at the internal one, the fatigue cracks are more inclined to initiate on the external surface despite the detrimental effect of the surface roughness of the internal surface on the fatigue strength. In this case, the fatigue cracks generally initiate along slip bands at the external surface of the specimens even though some intergranular fatigue crack initiations have been observed in a few cases. These observations are in accordance with the distribution of cracks according to the nature of the initiation site quantified by Mineur *et al.*[22] from fatigue tests conducted in air on a 316L steel loaded in fully reversed tension at a macroscopic plastic strain amplitude $E_a=2.10^{-3}$. In the case of specimens containing a hemispherical void, the initiation of the fatigue crack occurs along the surface of the void (Fig. 5),

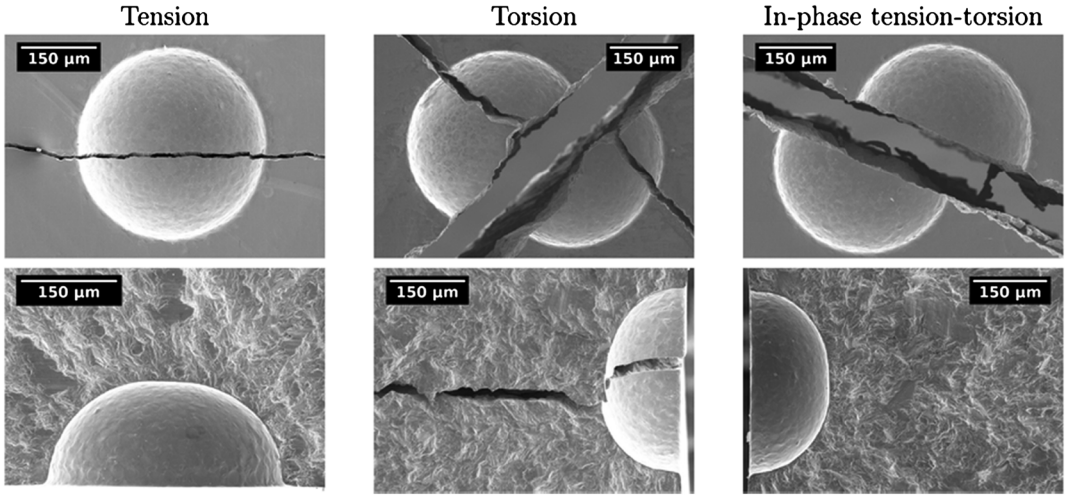

Fig. 5 Examples of external surfaces and fracture surfaces of specimens containing a hemispherical defect with a diameter $D = 365$ µm under fully reversed uniaxial tension, torsion and in-phase tension–torsion.

whatever the defect size investigated, except in the case of biaxial tension with a void diameter $D = 365$ µm for which one of the specimens failed because of the initiation of a fatigue crack on the internal surface, far from the void. Moreover, no local initiation site is clearly identifiable. Indeed, in all cases studied, the fatigue cracks seem to initiate homogeneously on the periphery of the void. Finally, it can be observed in Fig. 5 that the propagation of the fatigue cracks occurs macroscopically in the plane(s) perpendicular to the maximum principal stress direction. This conclusion applies for each defect size and each loading condition investigated. It should be noted that the plane perpendicular to the maximum principal stress direction varies during the cycle in the case of loading conditions including torsion. Three cases can be identified:

1. In fully reversed torsion, two planes are equivalent in terms of maximum principal stress, leading to the initiation of two fatigue cracks.
2. In fully reversed in-phase tension and torsion, even though there are two different planes perpendicular to the direction of the maximum principal stress during the cycle, the maximum principal stress is far greater in one plane than in the other one, leading to the propagation of the crack only in the predominating plane.
3. In fully reversed out-phase tension and torsion, an infinite number of planes are perpendicular to direction of the maximum principal stress during the cycle and, even though the maximum principal stress is not constant, it is sufficiently high to drive the crack to propagate in various planes leading to a tortuous macroscopic crack path.

FINITE ELEMENT MODEL

In order to reproduce numerically, in a reasonable computation time, the fatigue tests conducted in this study, a simplified geometry of the specimen is modelled, and FE simulations of polycrystalline aggregates are carried out. The first simplification is the use of a two-dimensional (2D) geometry instead of a three-dimensional (3D) one; the 3D hemispherical void is hence approximated by a circular hole. The second approximation consists in explicitly modelling the microstructure only in the notch area. An isotropic matrix embeds the polycrystal in order to avoid an overestimation of the stress concentration induced by the void. The use of an isotropic matrix is a common practice in studies of notched microstructures (see, e.g. Refs [10,13,23]).

The dimensions of the microstructure presented in Fig. 6 have been chosen so that a hole with diameter $D = 510$ µm can be inserted in the polycrystalline aggregate. Given these dimensions and the mean grain size, the smooth polycrystalline aggregate contains 3265 grains. The process used to generate the 2D polycrystalline aggregates geometries is described in Ref. [24]. The hole diameters D considered in the FE simulations are 0, 50, 95, 365 and 510 µm.

The FE mesh of the computer-aided design of the microstructure is generated using Gmsh.[25] Three-node triangular FEs, with linear interpolation and generalized plane strain hypothesis, are used. In order to estimate satisfactorily the mechanical responses averaged per grain, each grain is discretized in average with 75 elements that lead to an FE model, which includes the matrix, containing approximately 280 000 elements.

The orientation of the crystal frame of each grain, with respect to the reference frame of the polycrystalline

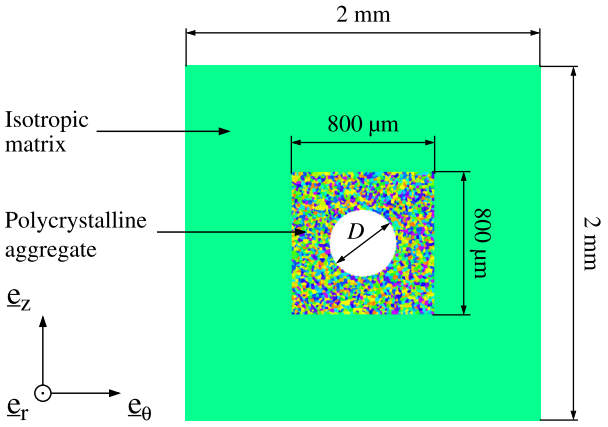

Fig. 6 Shape and dimensions of the polycrystalline aggregate and the matrix used in the finite element model.

aggregate, is defined by a triplet of Euler angles. Thus, orientation sets, composed by 3265 triplets of Euler angles, are constituted; the triplets of Euler angles being chosen such as to represent the crystallographic texture measured by X-ray diffraction on a region of the bar coinciding with the gauge section of the specimen. The methodology followed to select relevantly the triplets of Euler angles is the 'hybrid integer approximation' method proposed by Eisenlohr and Roters.[26] For each defect size studied, one geometry of polycrystalline aggregate and 10 orientations sets are used. As a result, the response of 10 different realizations is investigated per defect size.

A cubic elastic model, which describes the anisotropic elastic behaviour of face-centred cubic structures, is assigned to the grains. The crystal plasticity is omitted, which may seem questionable, especially in the case of microstructures containing a void. However, despite the drastic simplifications used to reduce the number of degrees of freedom, it is still significantly high, and given the number of realizations, loading conditions and defect sizes studied, the computations could not be achieved in a reasonable time if a crystal plasticity model is used. Nevertheless, several studies dealing with HCF account for the crystal plasticity in their modelling.[6–10,12,13,15,23,24] In particular, in Refs [12,13], the effect of the constitutive model on the mechanical responses and on the predictions of the probabilistic fatigue criterion discussed in the present study has been evaluated. An isotropic elastic model is used to define the behaviour of the matrix. The isotropic elastic moduli (Table 2) are determined with a tensile test, whereas those used in the cubic elastic model (Table 4) have been identified by Teklu *et al.* for an austenitic steel,[27] close to the one studied in the present work.

Homogeneous stress fields are applied to the edges of the matrix. The boundary conditions are chosen to model the loading conditions studied in the fatigue tests. It is worth noting that the torsion loading is approximated by a shear loading. Thanks to the linearity of the mechanical response and therefore to the superposition principle, the mechanical responses, over a complete cycle, are determined by combination of the mechanical fields computed using FE models with a unit stress applied on the matrix for three different macroscopic loadings: uniaxial tension Σ_{zz}, uniaxial tension $\Sigma_{\theta\theta}$ and shear $\Sigma_{\theta z}$. The numerical simulations are conducted with ZeBuLoN FE software (Transvalor, Evry, France).

Table 4 Elastic constants of the austenitic stainless steel at room temperature

	C_{1111} (GPa)	C_{1122} (GPa)	C_{1212} (GPa)	a
Cubic elastic constants of an Fe-18Cr-14Ni steel [20]	198	125	122	3.34
Isotropic elastic constants of the AISI 316L M25W steel	256	101	77	1.0

PROBABILISTIC FATIGUE CRITERION

Definition of the fatigue criterion

The probabilistic fatigue criterion presented in this section is inspired by a criterion proposed by Morel and Huyen[28] and has been the subject of studies dealing with an electrolytic copper.[12,13] Before detailing this criterion, it is worth noting that the mesoscopic mechanical quantities used in the criterion are computed from the stress tensors averaged per grain $\langle \underline{\sigma}(t) \rangle_g$, which are obtained at each time step t of the last loading cycle of the FE simulations of polycrystalline aggregates. In the present case, $t \in]0, T]$ with T the period of the loading cycle. The equations defining the mechanical quantities used in the probabilistic fatigue criterion are provided in the appendix.

In ductile metallic material, plastic strain is localized in the form of slip bands in some crystals favourably oriented with respect to the cyclic loading direction, leading to the formation, at the surface of the crystals, of intrusions and extrusions due to plastic slip irreversibility. Several experimental studies have shown that fatigue crack tends to initiate at the free surface along the interface between the slip band and the matrix (see, e.g. Ref. [29]). The formation of slip bands, whose understanding seems therefore essential to precisely predict the fatigue crack initiation, is governed by the dislocation structure resulting from complex interactions between dislocations, point defects and grain boundaries. The various mechanisms involved in the

formation of the dislocation structure are summarized in a thorough review of Sangid.[30] Some numerical modellings try to describe part of these mechanisms to predict the evolution of the dislocation structure from a given initial configuration. For example, a study conducted by Déprés *et al.*[31] has shown the capability of discrete dislocation dynamics simulations to reproduce heterogeneous dislocation microstructures similar to those observed in transmission electron microscopy (TEM) and the crucial role played by the cross slip in the dipole formation responsible for the irreversibility of the plastic strain localization. Although this approach is promising, its implementation in conjunction with FE analysis of polycrystalline aggregate remains difficult and would require excessive computation times. Thus, because the fatigue crack nucleation strongly depends on an underlying dislocation structure, which can hardly be determined in a polycrystal containing hundreds of grains, its modelling is considerably idealized in the present work.

The slip among grains being the main driving force of fatigue crack initiation in ductile alloys, it is natural to assume that the metallic polycrystals investigated in this study exhibit shear-dominated crack initiation, and thus, the amplitude of the shear stress acting on the slip planes is chosen to provide a coarse but sufficient measure of the slip activity. Moreover, as a positive normal stress acting on the slip plane facilitates the decohesion at the interface between the slip band and the matrix, it seems relevant to include this mechanical quantity in the fatigue criterion. Several studies carried out by the present authors[12,13] clearly showed that the shear stress and the normal stress, both acting on a slip plane, are strongly affected by the crystal orientation within the polycrystalline aggregate. The resulting statistical distributions over an arbitrary elementary volume of these quantities give a potential explanation of the experimental scatter of the macroscopic fatigue response usually observed in HCF. Nonetheless, as pointed out previously, the fatigue crack initiation remains a very complex mechanism, and the idealized modelling of the microstructure proposed in this work is unable to reflect all the local material heterogeneities and, in particular, the formation of dislocation structures leading to the localization of the plastic strain in slip bands. For these reasons, the formation of a fatigue crack at the scale of a single grain will be assumed to be governed not only by the mesoscopic shear and normal stresses acting on a slip plane (and deduced from the FE computations) but also affected by a statistical distribution of the crack initiation threshold assumed to be representative of the local microstructural heterogeneities. These microstructural heterogeneities have to be understood as the dislocation structures resulting from the evolution, through discrete mechanisms, of an unknown initial configuration of dislocations.

More practically, a fatigue crack is likely to appear in a grain if the shear stress amplitude τ_a acting on the most stressed plane exceeds a threshold τ_a^{th}. τ_a is defined as the radius of the smallest circle circumscribing the path Γ described by the mesoscopic shear stress vector $\underline{\tau}(\underline{n},t)$ acting on the slip plane $\underline{n}$ during the loading cycle (Fig 1b). A randomized algorithm, summarized in Ref. [32], is used to efficiently find the minimum enclosing circle of the path Γ of each slip plane in the microstructures.

The fatigue crack initiation threshold τ_a^{th} is then supposed to be a random variable following a Weibull distribution characterized by a shape parameter m and a scale parameter τ_0. Hence, the probability that a fatigue crack initiation occurs on a slip plane can be expressed by

$$P_{Fn} = P\left(\tau_a \geq \tau_a^{th}\right) = 1 - \exp\left[-\left(\frac{\tau_a}{\tau_0}\right)^m\right] \tag{2}$$

The mesoscopic normal stress acting on the slip plane of normal $\underline{n}$ is assumed to modify the initiation conditions by affecting the scale parameter. More precisely, the expression of τ_0 depends on the mesoscopic normal stress amplitude $\sigma_{n,a}$, through a triaxiality factor $\sigma_{n,a}/\tau_a$, and the mesoscopic mean normal stress $\sigma_{n,m}$:

$$\tau_0 = \tau_0{}' \frac{1 - \gamma\sigma_{n,m}}{1 + \alpha\left(\sigma_{n,a}/\tau_a\right)} \tag{3}$$

The failure probability P_{Fg} of a given grain is supposed to correspond to the maximum among the failure probabilities P_{Fn} of its slip planes. Finally, the failure probability of the polycrystalline aggregate P_{Fa} is computed according to the weakest-link hypothesis:

$$1 - P_{Fa} = \prod_{g=1}^{Ng}\left(1 - P_{Fg}\right) \tag{4}$$

where N_g is the number of grain constituting the polycrystalline aggregate. The use of the weakest-link hypothesis is justified by the fact that in HCF regime, the failure is driven by the initiation and the propagation of a single crack more than the initiation and the coalescence of a large number of cracks. It is worth noting that, because of the large number of grains contained in the polycrystalline aggregate, the failure probability of the polycrystalline aggregate P_{Fa} should be understood as the failure probability at the macroscopic scale.

Identification of the fatigue criterion parameters and prediction of the average fatigue limits

The fatigue criterion has four parameters which have to be identified:

- τ_0' describing the sensitivity of the fatigue limit to the mesoscopic shear stress amplitude τ_a;
- α describing the sensitivity of the fatigue limit to the mesoscopic normal stress amplitude $\sigma_{n,a}$;
- γ describing the sensitivity of the fatigue limit to the mesoscopic mean normal stress $\sigma_{n,m}$; and
- m describing the scatter of the fatigue limit and indirectly the sensitivity to the void.

These parameters cannot be identified analytically, so the results from the FE simulations of polycrystalline aggregates have to be used in the identification process. In these FE simulations, the polycrystalline aggregates are loaded at the average fatigue limit level, and the loading conditions applied on their matrix, during the identification, are chosen for their simplicity and so that to emphasize each mechanical quantity used in the fatigue criterion,

- fully reversed uniaxial tension and fully reversed shear lead to different triaxiality factors $\sigma_{n,a}/\tau_a$ enabling to identified the parameters τ_0' and α; and
- uniaxial tension with a loading ratio $R = 0.1$ induces mesoscopic mean normal stress $\sigma_{n,m}$ and thus allows the identification of the parameter γ.

A measure of the scatter of the fatigue limit (e.g. the standard deviation of the fatigue strength distribution) is needed to identify the shape parameter m. However, because of the lack of experimental data, it is not possible to estimate correctly the scatter of the fatigue limit. Therefore, the shape parameter is not identified but imposed, and two m values are chosen (5 and 20) in order to better understand the influence of this parameter on the distributions of the macroscopic fatigue limits predicted by the probabilistic criterion.

To sum up, the identification of the criterion parameters rely on the results of the numerical simulations on smooth microstructures loaded, at the average fatigue limit level, in uniaxial tension with $R = -1$ and $R = 0.1$ and in shear with $R = -1$. The average fatigue limits obtained with smooth specimen for these loading conditions can be found in Table 3. For each value of the shape parameter m, the parameters τ_0', α and γ are identified such that the failure probability of the aggregates P_{Fa} is, in average on the 10 realizations of microstructures, equal to 50% for each of the three loading conditions.

Once the parameters are identified, the fatigue criterion is used to predict the average fatigue limits for the other loading conditions and in the case of holed microstructures. For a given loading case and void diameter, the determination of the predicted average fatigue limit consists in searching the macroscopic stress amplitudes $\Sigma_{ij,a}$, which have to be applied to the matrix such as, in average on the 10 realizations, P_{Fa} is equal to 50%.

Prediction of the distribution of the macroscopic fatigue limits

Given the definition of the probabilistic fatigue criterion, it can be shown that, in the case where grains behaviour is linear and without any mesoscopic mean normal stress $\sigma_{n,a}$, the macroscopic fatigue limit $\Sigma_{ij,a}$ of a given microstructure follows a Weibull distribution (Eq. 5) whose shape parameter m^* is equal to the shape parameter m of the distribution of the fatigue crack initiation threshold τ_a^{tb}:

$$f_a(\Sigma_{ij,a}) = \frac{m^*}{\tau_0^*}\left(\frac{\Sigma_{ij,a}}{\tau_0^*}\right)^{m^*-1} \exp\left[-\left(\frac{\Sigma_{ij,a}}{\tau_0^*}\right)^{m^*}\right] \quad (5)$$

The scale parameter τ_0^* characterizing the distribution of the macroscopic fatigue limit $\Sigma_{ij,a}$ can be identified, for example, from the macroscopic fatigue limit $\Sigma_{ij,a}^{P_{Fa}=50\%}$, that is, the loading amplitude for which the failure probability of the aggregate P_{Fa} is equal to 50%, using the following relation:

$$\tau_0^* = \frac{\Sigma_{ij,a}^{P_{Fa}=50\%}}{\ln\,(2)^{1/m^*}} \quad (6)$$

It is worth noting that the parameter τ_0^*, because of its relation with the macroscopic fatigue limit $\Sigma_{ij,a}^{P_{Fa}=50\%}$, depends on the microstructure. Thus, the probability density function f_a, which represents the distribution of the macroscopic fatigue limit induced by the distribution of the fatigue crack initiation threshold τ_a^{tb}, is also dependent on the realization. In particular, in the case of holed microstructures, it seems reasonable to suppose that the configuration of the grain orientations in the vicinity of the hole affects significantly this distribution. Therefore, the distribution of the macroscopic fatigue limit, taking into account the variability of the microstructure, can be characterized by the probability density function $f_{average}$ defined as the average of the probability density functions f_a:

$$f_{average} = \frac{1}{N_r}\sum_{a=1}^{N_r} f_a \quad (7)$$

with N_r corresponding to the number of realizations. An example of the probability density functions f_a and the average probability density function $f_{average}$, obtained with a shape parameter $m = 20$ in the case of microstructures containing a hole of diameter $D = 50\,\mu m$ and loaded in fully reversed tension, is presented in Fig. 7.

RESULTS AND DISCUSSION

Predictions of the average fatigue limits

The average macroscopic fatigue limits $\Sigma_{ij,a}$ predicted by the probabilistic fatigue criterion are presented, along with those determined from the fatigue tests results, in a diagram $\Sigma_{ij,a}$–D in Fig. 8 for shape parameters $m = 5$ and $m = 20$. The macroscopic stress amplitude $\Sigma_{ij,a}$ considered to represent the macroscopic fatigue limit is the axial macroscopic stress $\Sigma_{zz,a}$ excepted in the case of the torsion loading for which the macroscopic fatigue limit is defined by the macroscopic shear stress $\Sigma_{\theta z,a}$.

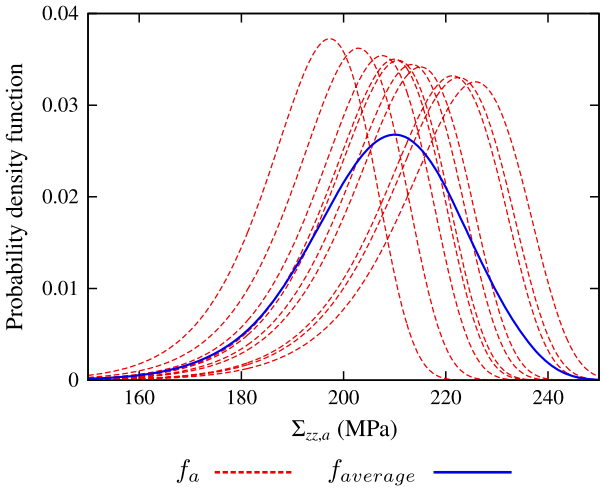

Fig. 7 Probability density functions f_a describing the distribution of the failure probability of polycrystalline aggregates loaded in fully reversed tension and the average probability density function $f_{average}$ describing the distribution of the macroscopic fatigue limit.

In the absence of voids and whatever the value of the shape parameter m, the predictions of the probabilistic fatigue criterion are in good accordance with the experimental average fatigue limits, excepted for the combined tension and torsion with a phase shift $\varphi_{\theta z} = 90°$. Indeed, in this latter case, the difference between the experimental and predicted fatigue limits is approximately 22%. Moreover, it is worth noting that the predictions are conservative when the aggregates are defect-free.

In the presence of a void, the quality of the predictions is more fluctuating and depends on the value of the shape parameter m, the best estimates being obtained for a shape parameter $m = 5$ among the values studied (two others values, whose results are not presented, were tested: 10 and 15). Indeed, for greater value of the shape parameter, the detrimental influence of the void on the fatigue strength is overestimated, thus leading to predictions significantly conservatives.

In order to understand the effect of the shape parameter m on the average fatigue limits predicted by the probabilistic fatigue criterion, it is interesting to visualize the distributions of the failure probability P_{Fg} of the grains in a microstructure for different defect sizes D. These distributions are illustrated in Fig. 9 for a microstructure loaded in fully reversed tension. The results obtained with shape parameters $m = 5$ and $m = 20$ are presented, respectively, in Fig 9a and b. The same orientation set is used in each model; only the void diameter D varies in the first, second, third and fourth columns are exposed the microstructures containing a hole with a diameter D equal to, respectively, 0, 50, 95 and 365 µm. It can be observed that, in the absence of void, the distribution of the failure probability of the grains P_{Fg} is heterogeneous because of the anisotropy of the grains'

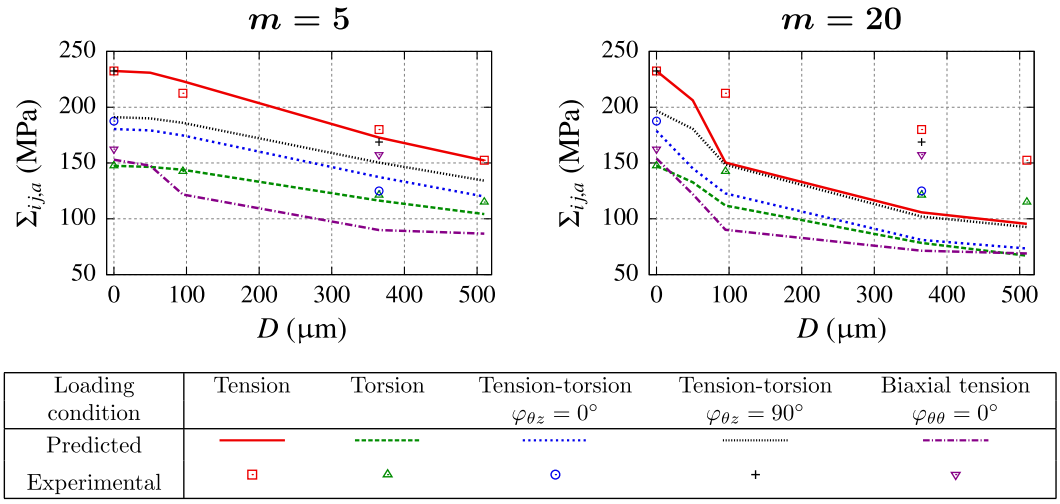

Fig. 8 Comparison between the average fatigue limits determined experimentally and those predicted by the probabilistic fatigue criterion with $m = 5$ and $m = 20$.

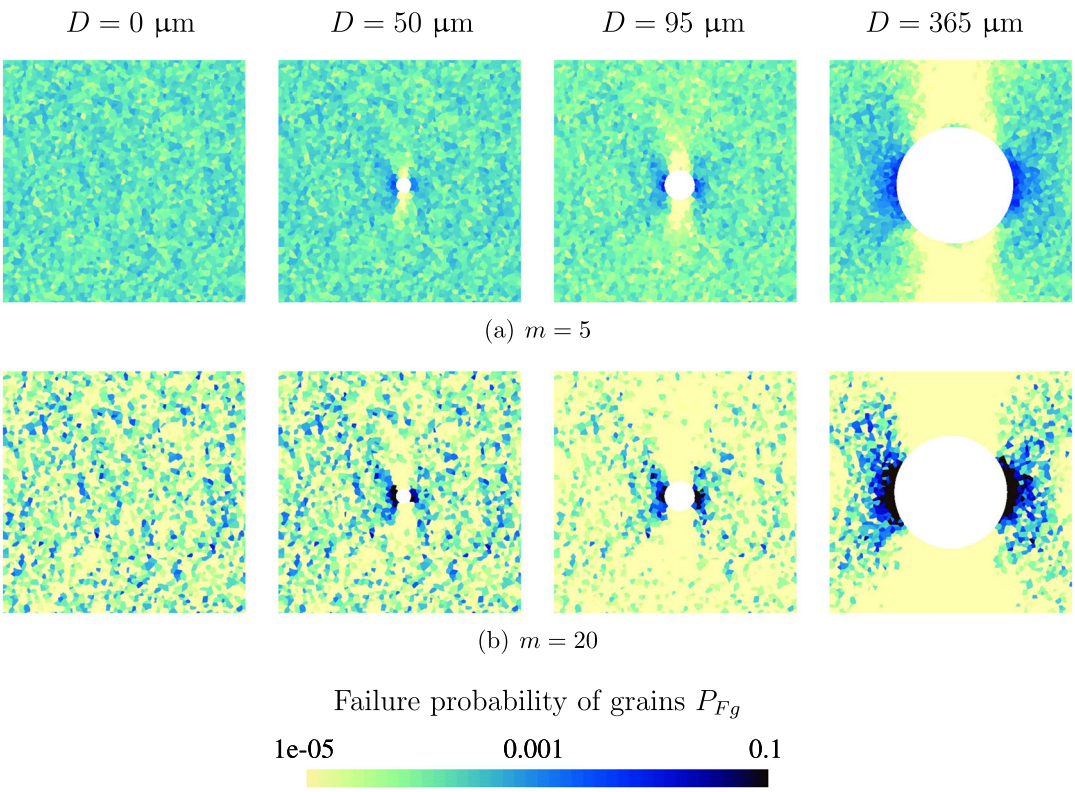

Fig. 9 Distribution of the failure probabilities of the grains $P_{F,g}$ in a microstructure loaded in fully reversed uniaxial tension at the experimental average fatigue limit level for different defect diameters D and shape parameters m.

behaviour and their crystalline orientations leading to heterogeneous mechanical responses. Moreover, the addition of a void in the polycrystalline aggregate increases the heterogeneity of the failure probability P_{Fg} because of the stress concentration induced in the vicinity of the defect. It also appears that in the case of a shape parameter $m = 5$, the distribution of the failure probability P_{Fg} is more homogeneous than in the case of a shape parameter $m = 20$. Thus, it can be concluded that, even though all the grains in the microstructure are considered to predict the failure probability P_{Fa} of the aggregate, the contribution of each grain to the fatigue failure is driven by the parameters of the Weibull distribution defining the fatigue crack initiation threshold. The lower the shape parameter m, the higher the contribution to the failure of the most stressed grains and the lower the less stressed grains contribute to the failure.

In order to ease the comparison between the experimental data and the best estimates of the criterion (obtained in the case where the shape parameter $m = 5$), the relative differences between the experimental fatigue limits and those predicted by the probabilistic fatigue criterion are computed and presented in Table 5. The relative difference is defined in function of the average fatigue limits determined experimentally $\Sigma_{ij,a}^{exp}$ and predicted $\Sigma_{ij,a}^{pred}$ in the following way:

$$Difference = \frac{\Sigma_{ij,a}^{exp} - \Sigma_{ij,a}^{pred}}{\Sigma_{ij,a}^{exp}} \quad (8)$$

With this definition, a positive difference corresponds to a conservative prediction, whereas a negative difference is a sign of a too optimistic prediction. It can be observed that the difference between the experimental fatigue limits and the predictions does not exceed 10% in the case of the tension, torsion and in-phase tension and torsion loadings for every defect diameters studied. The predictions are less satisfactory in the case of the combined tension and torsion with a phase shift $\varphi_{\theta z} = 90°$. Indeed, for this loading condition and for the considered void diameters D, the differences range from 10 to 20%. However, these predictions have the merit of being conservative. Finally, the accuracy of the predicted fatigue limits in the case of in-phase biaxial tension with a loading ratio $R = 0.1$ and a biaxiality ratio $k_{\theta z} = 0.5$ [0, 1] is very variable: in the absence of void, the macroscopic fatigue limit is predicted satisfactorily, whereas in the presence of a hole with a diameter $D = 365$ µm, the decrease of the fatigue limit is largely overestimated by the probabilistic fatigue criterion. In this latter case, a difference between the prediction and the experimental fatigue limit greater than 20% is observed. Nevertheless, the inaccuracy of the probabilistic criterion to predict

Table 5 Values of the relative differences between the average fatigue limits determined experimentally $\Sigma_{ij,a}^{exp}$ and predicted $\Sigma_{ij,a}^{pred}$ with a shape parameter $m = 5$ for each loading conditions and each defect diameter D

Loading condition	D (μm)	$\Sigma_{ij,a}^{exp}$ (MPa)	$\Sigma_{ij,a}^{pred}$ (MPa)	Difference (%)
Uniaxial tension $R = -1$	0	233	233	0
	95	213	223	−5
	365	180	173	4
	510	153	152	0
Torsion $R = -1$	0	148	148	0
	95	143	144	1
	365	121	116	4
	510	115	104	9
Tension–torsion $R = -1$, $k_{\theta z} = 0.5$, $\varphi_{\theta z} = 0°$	0	188	180	4
	365	120	137	−10
Tension–torsion $R = -1$, $k_{\theta z} = 0.5$, $\varphi_{\theta z} = 90°$	0	233	191	18
	365	169	150	11
Biaxial tension $R = -1$, $k_{\theta\theta} = 0.5$, $\varphi_{\theta\theta} = 0°$	0	163	153	6
	365	157	90	43

the fatigue strength in the case of a biaxial tensile loading in the presence of a void has to be tempered, given the fact that the fatigue limit determined experimentally is questionable for this configuration. Indeed, for this loading condition and this defect size, the average fatigue limit has been estimated with only two specimens for this configuration.

Scatter of the fatigue limits

The probability density functions $f_{average}$ predicted by the probabilistic fatigue criterion for each defect diameter D are illustrated in Fig. 10 for different loading conditions. In this figure, the first and second columns contain the predictions obtained, respectively, with a shape parameter $m = 5$ and $m = 20$. It is worth noting that, in the absence of void, the macroscopic fatigue limits can be correctly approximated by a Weibull probability density function. This observation is no longer valid when the microstructures contain a hole because of the irregularities encountered in the distributions of the macroscopic fatigue limits. It seems reasonable to assume that this lack of regularity in the distributions of the macroscopic limit is due to an insufficient number of microstructures to describe the variety of possible configurations of crystalline orientations in the vicinity of small holes. The quantitative comparison between the results obtained for different hole diameters D and loading conditions is complicated by the inability to describe the probability densities $f_{average}$ by a usual and unique probability law. For these reasons, the discussion on the distributions is only qualitative. From the results, it appears that, for a shape parameter $m = 5$, an increase in the diameter D of the circular hole from 0 to 510 μm leads to a progressive decrease in the scatter of the average macroscopic fatigue limits, whatever the loading condition considered. The trends are different in the case of a shape parameter $m = 20$. Indeed, circular holes with diameters $D = 50$ μm and $D = 95$ μm increase generally the scatter of the fatigue limits, whereas for D greater than 95 μm, an increase in the hole diameter induces a decrease in the scatter of the fatigue strength.

It is important to remind that the best predictions of the average fatigue limits are obtained with a shape parameter $m = 5$. For this value, it appears that the ratio between the standard deviation and the average macroscopic fatigue limit $\Sigma_{zz,a}$ in fully reversed tension is approximately equal to 0.23 in the absence of void. However, in a 304L austenitic steel, relatively close to the 316L steel studied, this ratio is estimated at 0.05 (Ref. [33]). Thus, it seems that the probabilistic criterion strongly overestimates the scatter of the fatigue limit. In the case of a shape parameter $m = 20$, the scatter of the macroscopic fatigue limit predicted by the criterion is in better accordance with the one observed experimentally on a 304L steel in fully reversed tension, but the influence of the void on the decrease in the average macroscopic fatigue limits is significantly overestimated. In these conditions, the identification process discussed previously seems compromised. The proposed methodology consists in identifying the shape parameter m so that the standard deviation of the macroscopic fatigue limit predicted by the criterion for a given loading condition fits to the one observed experimentally. Unfortunately, according to these results, it seems difficult to conciliate satisfactory predictions of the average macroscopic fatigue limits in the presence of voids with a correct estimate of the scatter of the fatigue limits. Nevertheless, it is important to keep in mind that some strong assumptions have been used to predict the distributions of the macroscopic fatigue limits, and the fatigue criterion is not necessarily the main cause of the incompatibility of the predictions, in terms of average and scatter. Among the hypotheses used, the omission of the crystal plasticity

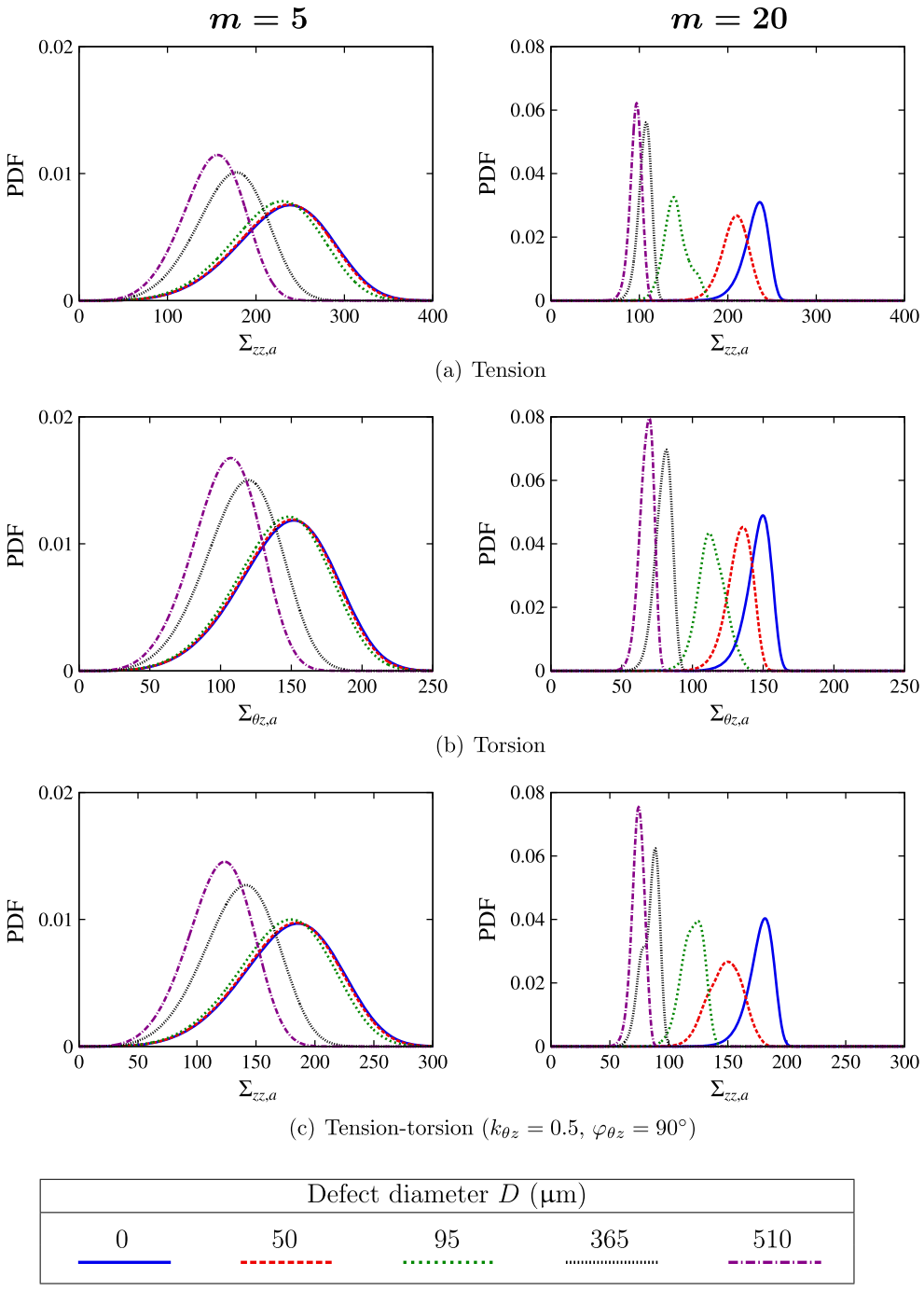

Fig. 10 Probability density functions describing the macroscopic fatigue limit distributions for each defect size studied and for different loading conditions: (a) tension, (b) torsion and (c) in-phase tension–torsion.

is certainly one of the most influential on the distribution of the mesoscopic mechanical quantities, especially in the presence of a void, and consequently, it may affect the predictions of the fatigue criterion. For example, in Ref. [13], the effect of the crystal plasticity on the average fatigue limits predicted by the probabilistic fatigue criterion has been evaluated, and it has been shown that, for a shape parameter $m = 20$, the addition of the crystal plasticity leads to an increase of the average fatigue limits in the presence of voids. Therefore, taking into account the crystal plasticity in the grain's constitutive model might provide more consistent predictions. A thorough investigation of the effect of the crystal plasticity on the predictions would deserve to be carried out in order to

estimate to which extent the omission of this behaviour is responsible for the inability to conciliate the average and the scatter of the fatigue limits predicted by the probabilistic fatigue criterion.

SUMMARY AND CONCLUSIONS

Experimental tests have been performed on a 316L austenitic steel in order to characterized its mechanical and metallurgical properties. In particular, a series of constant stress amplitude fatigue tests has been carried out to estimate the average fatigue limits at 2.10^6 cycles of this steel under various loading conditions (uniaxial tension with $R=-1$ and $R=0.1$, torsion with $R=-1$, combined tension and torsion with $R=-1$ and with $\varphi_{\theta z}=0°$ and $\varphi_{\theta z}=90°$ and in-phase biaxial tension with $R=0.1$). The tests have been conducted on tubular specimen containing, on the external surface, an artificial hemispherical void and on defect-free specimen. The diameters D of the hemispherical voids studied are 95, 365 and 510 µm. These void sizes did not allow highlighting an eventual critical defect size, under which the fatigue limit is not affected by the void, whatever the loading condition imposed on the specimen. However, it has been shown that some trends observed on metallic material are verified by the 316L austenitic steel. Especially, the detrimental influence of the void is more pronounced in fully reversed tension than in fully reversed torsion. Concerning the results of the fatigue tests under multiaxial loading conditions, two interesting facts have been pointed out: the beneficial effects, on the fatigue strength, of the increase of the phase shift $\varphi_{\theta z}$, from 0° to 90°, in the case of combined tension and torsion and of the increase of the biaxiality ratio $k_{\theta\theta}$, from 0 to 0.5, in the case of biaxial tension.

In a second step, a numerical study has been carried out in order to predict the distribution of the fatigue limits for several defect sizes and loading conditions. This study relies on FE simulations of polycrystalline aggregates, which allow estimating the stress tensors averaged per grain and, therefore, the mechanical quantities used in a probabilistic fatigue criterion. The average macroscopic fatigue limits are correctly predicted by the fatigue criterion, with a simplified 2D modelling of the microstructure, in the case of fully reversed tension, fully reversed torsion and fully reversed in-phase tension and torsion. In the case of combined tension and torsion with a phase shift $\varphi_{\theta z}=90°$, the relative differences between the experimental and the predicted fatigue limits turn out to be more substantial, but the predictions are conservatives. The predictions are more spread out in the case of biaxial tension: in the absence of void, the average fatigue limit is satisfactorily predicted by the fatigue criterion, whereas in the presence of a void with diameter $D=365$ µm, a relative difference of 43% is encountered.

The distribution of the macroscopic fatigue limit has also been estimated by the probabilistic fatigue criterion and has been studied for different defect diameters and loading conditions. The scatter of the macroscopic fatigue limit seems generally overestimated when the criterion is identified such as to correctly predict the average fatigue limit. By changing the shape parameter m of the Weibull distribution describing the fatigue crack initiation threshold in order to predict a more reasonable scatter, it appears that this latter is sensitive to the void size. Indeed, circular holes with diameters $D=50$ µm and $D=95$ µm increase generally the scatter of the fatigue limits. This increase can be attributed to the lack of representativeness of the crystalline orientations in the small region affected by the void. On the contrary, for D greater than 95 µm, an increase in the hole diameter induces a decrease in the scatter of the fatigue strength. Nevertheless, it is worth noting that this trend has not been confirmed experimentally because of an insufficient number of specimens used in the series of fatigue tests.

Even though a simplified modelling of microstructures (use of 2D geometries and omission of the crystal plasticity) has allowed obtaining satisfactory predictions, at least concerning the average macroscopic fatigue limits for different void sizes and loading conditions, it could be interesting to evaluate the consequences of these simplifications on the mesoscopic mechanical responses and on the predictions of the probabilistic criterion. These analyses can be performed by comparing the current results with those obtained with more realistic 3D microstructure accounting for the crystal plastic. These questions will be addressed in a forthcoming paper.

Acknowledgements

The authors gratefully acknowledge the technical support provided by Daniel Cuillerier and Instron®, in particular Sébastien Picard, during the fatigue tests setting up.

REFERENCES

1 Murakami Y. and Endo M. (1994) Effects of defects, inclusions and inhomogeneities on fatigue strength. *Int. J. Fatigue*, **16**, 163–182.
2 Auricchio F., Constantinescu A. and Scalet G. (2014) Fatigue of 316L stainless steel notched µm-size components. *Int. J. Fatigue*, **68**, 231–247.
3 Susmel L. and Taylor D. (2006) A simplified approach to apply the theory of critical distance to notched components under torsional fatigue loading. *Int. J. Fatigue*, **28**, 217–230.

4 Endo M. and Ishimoto I. (2006). The fatigue strength of steels containing small holes under out-of-phase combined loading. *Int. J. Fatigue*, **28**, 592–597.
5 Askes H., Livieri P., Susmel L., Taylor D. and Tovo R. (2013) Intrinsic material length theory of critical distances and gradient mechanics: analogies and differences in processing linear-elastic crack tip stress fields. *Fatigue Fract. Eng. Mater. Struct.*, **36**, 39–55.
6 Bennett V. and McDowell D. (2003) Polycrystal orientation distribution effects on microslip in high cycle fatigue. *Int. J. Fatigue*, **25**, 27–39.
7 Guilhem Y., Basseville S., Curtit F., Stéphan J. M. and Cailletaud G. (2010) Investigation of the effect of grain clusters on fatigue crack initiation in polycrystals. *Int. J. Fatigue*, **32**, 1748–1763.
8 Fang X., Yan W., Gao H., Yue Z., Liu J. and Wang F. (2012) Finite element simulation of surface deformation of polycrystal with a rough surface under repeated load. *Finite Elem. Anal. Des.*, **60**, 64–71.
9 Le Pécheur A., Curtit F., Clavel M., Stephan J., Rey C. and Bompard P. (2012) Polycrystal modelling of fatigue: pre-hardening and surface roughness effects on damage initiation for 304L stainless steel. *Int. J. Fatigue*, **45**, 48–60.
10 Owolabi G., Prasannavenkatesan R. and McDowell D. (2010) Probabilistic framework for a microstructure-sensitive fatigue notch factor. *Int. J. Fatigue*, **32**, 1378–1388.
11 Charkaluk E., Constantinescu A., Szmytka F. and Tabibian S. (2014) Probability density functions: from porosities to fatigue lifetime. *Int. J. Fatigue*, **63**, 127–136.
12 Guerchais R., Robert C., Morel F., and Saintier N. (2014). Micromechanical study of the loading path effect in high cycle fatigue. *Int. J. Fatigue*, **59**, 64–75.
13 Guerchais R., Saintier N., Morel F., and Robert C. (2014) Micromechanical investigation of the influence of defects in high cycle fatigue. *Int. J. Fatigue*, **67**, 159–172.
14 Argente dos Santos H. A. F., Auricchio F. and Conti M. (2012) Fatigue life assessment of cardiovascular balloon-expandable stents: a two-scale plasticity–damage model approach. *J. Mech. Behavior Biomedical Mater.*, **15**, 78–92.
15 Sweeney C. A., McHugh P. E., McGarry J. P. and Leen S. B. (2012) Micromechanical methodology for fatigue in cardiovascular stents. *Int. J. Fatigue*, **44**, 202–216.
16 Wiersma S. and Taylor D. (2005) Fatigue of materials used in microscopic components. *Fatigue Fract. Eng. Mater. Struct.*, **28**, 1153–1160.
17 Donnelly E. (2012). Geometry effect in the fatigue behavior of microscale 316L stainless steel specimens. PhD thesis, National University of Ireland.
18 Bachmann F., Hielscher R. and Schaeben H. (2010) Texture analysis with MTEX-free and open source software toolbox. *Solid State Phenomena*, **160**, 63–68.
19 Endo M. and Murakami Y. (1987) Effects of an artificial small defect on torsional fatigue strength of steels. *J. Eng. Mater. Technol.*, **109**, 124–129.
20 Murakami Y., Matsunaga H., Abyazi A. and Fukushima Y. (2013) Defect size dependence on threshold stress intensity for high-strength steel with internal hydrogen. *Fatigue Fract. Eng. Mater. Struct.*, **36**, 836–850.
21 Billaudeau T., Nadot Y. and Bezine G. (2004). Multiaxial fatigue limit for defective materials: mechanisms and experiments. *Acta Mater.*, **52**, 3911–3920.
22 Mineur M., Villechaise P. and Mendez J. (2000). Influence of the crystalline texture on the fatigue behavior of a 316L austenitic stainless steel. *Mater. Sci. Eng. A*, **286**, 257–268.
23 Bertolino G., Constantinescu A., Ferjani M. and Treiber P. (2007). A multiscale approach of fatigue and shakedown for notched structures. *Theor. Appl. Fract. Mech.*, **48**, 140–151.
24 Robert C., Saintier N., Palin-Luc T. and Morel F. (2012) Micro-mechanical modelling of high cycle fatigue behavior of metals under multiaxial loads. *Mech. Mater.*, **55**, 112–129.
25 Geuzaine C. and Remacle J. F. (2009). Gmsh: a 3D finite element mesh generator with built-in pre- and post-processing facilities. *Int. J. Numer. Meth. Eng.*, **79**, 1309–1331.
26 Eisenlohr P. and Roters F. (2008). Selecting a set of discrete orientations for accurate texture reconstruction. *Comp. Mater. Sci.*, **42**, 670–678.
27 Teklu A., Ledbetter H., Kim S., Boatner A., McGuire M. and Keppens V. (2004) Single-crystal elastic constants of Fe-15Ni-15Cr alloy. *Metall. Mater. Trans. A*, **35**, 3149–3154.
28 Morel F. and Huyen N. (2008) Plasticity and damage heterogeneity in fatigue. *Theor. Appl. Fract. Mech.*, **49**, 98–127.
29 Basinski Z. S. and Basinski S. J. (1992). Fundamental aspects of low amplitude cyclic deformation in face-centred cubic crystals. *Prog. Mater. Sci.*, **36**, 89–148.
30 Sangid M. D. (2013). The physics of fatigue crack initiation. *Int. J. Fatigue*, **57**, 58–72.
31 Déprés C., Robertson C. F. and Fivel M. C. (2004) Crack initiation in fatigue: experiments and three-dimensional dislocation simulations. *Mater. Sci. Eng. A*, **387–389**, 288–291.
32 Bernasconi A. and Papadopoulos I. (2005). Efficiency of algorithms for shear stress amplitude calculation in critical plane class fatigue criteria. *Comp. Mater. Sci.*, **34**, 355–368.
33 Malésys N. (2007) Modélisation probabiliste de formation de réseaux de fissures de fatigue thermique. PhD thesis, Ecole Normale Supérieure de Cachan.

APPENDIX

DEFINITIONS OF THE MECHANICAL QUANTITIES USED IN THE PROBABILISTIC FATIGUE CRITERION

The aim of this appendix is to detail the mathematical relationships allowing to compute the mechanical quantities used in the probabilistic fatigue criterion, namely, the amplitude of the shear stress $\tau_a(\underline{n})$, the amplitude of the mean normal stress $\sigma_{n,a}(\underline{n})$ and the mean normal stress $\sigma_{n,m}(\underline{n})$, both acting on a given slip plane Δ defined by its unit normal vector $\underline{n}$. It is worth noting that in a face-centred cubic crystal structure, the slip planes correspond to the set of planes {111}. The mechanical quantities are computed for a given grain, using the mesoscopic stress tensor $\langle \underline{\underline{\sigma}}(t) \rangle_g$, that is, the stress tensor averaged over the grain, with $t \in]0, T]$. Knowing the mesoscopic stress tensor $\langle \underline{\underline{\sigma}}(t) \rangle_g$ at time t, one can determine the stress vector $\underline{\sigma}(\underline{n}, t)$ acting on a given slip plane using the following equation:

$$\underline{\sigma}\left(\underline{n}, t\right) = \left\langle \underline{\underline{\sigma}}(t) \right\rangle_g . \underline{n} \tag{A.1}$$

It should be noted that it is essential to express vectors and tensors in the same basis in order to carry out correctly these computations.

The mesoscopic stress vector $\underline{\sigma}(\underline{n},t)$ can be decomposed into two vectors: the normal stress vector $\underline{\sigma}_{\mathrm{n}}(\underline{n},t)$ and the shear stress vector $\underline{\tau}(\underline{n},t)$, which are defined respectively in Eqs A.2 and A.3:

$$\underline{\sigma}_{\mathrm{n}}\left(\underline{n},t\right)=\left[\underline{\sigma}\left(\underline{n},t\right).\underline{n}\right]\ \underline{n}=\sigma_{\mathrm{n}}\left(\underline{n},t\right)\underline{n} \tag{A.2}$$

$$\underline{\tau}\left(\underline{n},t\right)=\underline{\sigma}\left(\underline{n},t\right)-\underline{\sigma}_{\mathrm{n}}\left(\underline{n},t\right) \tag{A.3}$$

In high-cycle fatigue, the strains are sufficiently small to ensure that the direction of the vector $\underline{n}$ and thus the direction of the normal stress vector $\underline{\sigma}_{\mathrm{n}}(\underline{n},t)$ remain constant during the loading cycle. In this case, the amplitude of normal stress $\sigma_{\mathrm{n,a}}(\underline{n})$ and the mean normal stress $\sigma_{\mathrm{n,m}}(\underline{n})$ can be easily expressed as follows:

$$\sigma_{\mathrm{n,a}}\left(\underline{n}\right)=\frac{1}{2}\left(\max_{t\in[0,T]}\left[\sigma_{\mathrm{n}}\left(\underline{n},t\right)\right]-\min_{t\in[0,T]}\left[\sigma_{\mathrm{n}}\left(\underline{n},t\right)\right]\right) \tag{A.4}$$

$$\sigma_{\mathrm{n,m}}\left(\underline{n}\right)=\frac{1}{2}\left(\max_{t\in[0,T]}\left[\sigma_{\mathrm{n}}\left(\underline{n},t\right)\right]+\min_{t\in[0,T]}\left[\sigma_{\mathrm{n}}\left(\underline{n},t\right)\right]\right) \tag{A.5}$$

Unlike the normal stress vector $\underline{\sigma}_{\mathrm{n}}\left(\underline{n},t\right)$, the direction of the shear stress vector $\underline{\tau}(\underline{n},t)$ is not necessarily constant during the loading cycle. Therefore, the shear stress vector $\underline{\tau}(\underline{n},t)$ acting on the slip plane may describe a path Γ in the plane Δ (Fig 1b). Under these conditions, the definitions of the amplitude of the shear stress $\tau_{\mathrm{a}}(\underline{n})$ and the mean shear stress $\tau_{\mathrm{m}}(\underline{n})$ are less obvious than in the case of the normal stress. Among the possible definitions of $\tau_{\mathrm{a}}(\underline{n})$ and $\tau_{\mathrm{m}}(\underline{n})$, the one based on the minimum circumscribed circle encompassing the path Γ is chosen (Ref. [32]). In this case, the amplitude of the shear stress $\tau_{\mathrm{a}}(\underline{n})$ is defined by the radius of the smallest circle circumscribing the path Γ, and the vector defined by the origin of the shear stress vector and the centre of this circle correspond to the mean shear stress vector $\underline{\tau}_{\mathrm{m}}(\underline{n})$. Finding the centre of the minimum circumscribed circle encompassing the path Γ is a minimization problem, which can be formulated as follows:

$$\underline{\tau}_{\mathrm{m}}\left(\underline{n}\right)=\underset{\underline{\tau}'\left(\underline{n}\right)\in\Delta}{\operatorname{argmin}}\left[\max_{t\in[0,T]}\left\|\underline{\tau}\left(\underline{n},t\right)-\underline{\tau}'\left(\underline{n}\right)\right\|\right] \tag{A.6}$$

Once the centre is determined, the radius $\tau_{\mathrm{a}}(\underline{n})$ of the smallest circle circumscribing the path Γ is computed using the following relationship:

$$\tau_{\mathrm{a}}\left(\underline{n}\right)=\max_{t\in[0,T]}\left\|\underline{\tau}\left(\underline{n},t\right)-\underline{\tau}_{\mathrm{m}}\left(\underline{n}\right)\right\| \tag{A.7}$$

This shear stress amplitude $\tau_{\mathrm{a}}\left(\underline{n}\right)$ must not be mistaken for the resolved shear stress amplitude acting along a given slip direction, that is, the amplitude based on the projection of the shear stress vector $\underline{\tau}(\underline{n},t)$ on a slip direction defined by its unit normal vector $\underline{l}$.